

High-performance Single Photon Avalanche Diodes for QKD Networks

Mark A. Itzler, Xudong Jiang, Bruce Nyman, and Krysl Slomkowski
Princeton Lightwave Inc., 2555 US Route 130 S., Cranbury, NJ 08540 USA
[e-mail: mitzler@princetonlightwave.com]

Abstract

We describe recent results for the performance and modeling of InP-based single photon avalanche diodes designed for use at 1.5 μm . Dark count probabilities (DCP) as low as 5×10^{-7} per ns have been achieved at 215 K for a photon detection efficiency (PDE) of 10%, and $\text{DCP} \sim 1 \times 10^{-6}$ per ns has been obtained for PDE as high as 25%. We also report the dependence of afterpulsing on repetition rates up to 10 MHz, as well as modeling of the dependence of dominant dark carrier generation mechanisms on conditions such as temperature and bias.

Introduction

Single photon detectors are often the most critical components constraining the overall performance of quantum key distribution (QKD) networks. From the perspective of performance, cost, and reliability, InP-based single photon avalanche diodes (SPADs) are the most promising detector technology for widespread deployment in QKD systems. In this paper, we describe our progress in improving the performance of InP-based SPADs. We present characterization data demonstrating a very low dark count probability (DCP) of 5×10^{-7} per ns for a photon detection efficiency (PDE) of 10% at 215 K. We also illustrate the dependence of DCP on gate repetition rate and show that afterpulsing remains below 10^{-4} for repetition rates up to 5 MHz for a PDE of 10%. Finally, we describe detailed modeling with which we have quantified the dominant dark carrier generation mechanisms and obtained a more comprehensive understanding of SPAD behavior given changes in operating conditions such as temperature and applied bias.

Trade-off between DCP and PDE

Our basic SPAD design relies on the use of an InGaAs absorption region lattice-matched to InP substrates, combined with an InP multiplication region in a canonical separate absorption and multiplication (SAM) region avalanche diode structure. A thorough description of the device structure can be found in Ref. [1]. SPADs are operated in “Geiger-mode” by gating the applied bias V above the breakdown voltage V_b by an excess bias V_{ex} (i.e., $V_{\text{ex}} = V - V_b$). In this operating mode, a single photoexcited carrier can give rise to a macroscopic avalanche of charge which is detectable in a purely digital fashion using an appropriate threshold detection circuit. After detection, the avalanche is quenched using an appropriate quenching circuit [2].

The most fundamental trade-off in SPAD performance occurs in trying to maximize PDE while minimizing DCP. PDE is the probability of an incoming photon generating a photoexcited carrier that is successfully detected. DCP is the probability

that a carrier created by any mechanism other than photoexcitation (i.e., a dark carrier) is detected. PDE is increased by applying a larger V_{ex} since the probability P_a of inducing a detectable avalanche is enhanced by the associated increase in internal electric field. However, any increase in P_a is accompanied by a proportional increase in DCP. Moreover, if DCP has significant contributions from field-dependent dark carrier excitation mechanisms, it will exhibit an even faster rise with increasing V_{ex} compared to the rise in PDE.

To the extent that dark carrier generation is mediated by defects, good epitaxial material quality is critical to achieving low DCP. Beyond the base material quality, precise control of the internal electric field through epitaxial layer design is essential for minimizing field-induced dark carriers. Through successive design iterations and comprehensive modeling (described below), we have made substantial improvements in the DCP vs. PDE trade-off for 1.5 μm SPADs.

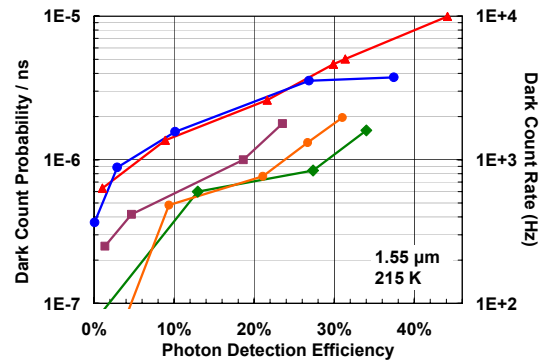


Figure 1: DCP per 1-ns gate vs. PDE for five SPADs with a 25- μm optical diameter.

In Figure 1, we illustrate DCP vs. PDE data for five SPADs taken from a recent production fabrication run. The devices have a 25- μm optical diameter and were fiber-coupled in a 14-pin butterfly package. Device-to-device performance variations exist due to local variations in material quality and epitaxial structure, but the best of these devices achieve a $\text{DCP} \sim 5 \times 10^{-7}$ per ns for a 10% PDE

(commonly used in QKD networks) at a temperature of 215 K obtained using thermoelectric coolers.

Each data point in Figure 1 was obtained by measuring DCP and PDE at a fixed value of V_{ex} using short 1-ns gates with a repetition rate of 500 kHz [3]. The bias circuitry has a fixed voltage swing $\Delta V \sim 4$ V. Proper operation results when a dc bias $V_{dc} < V_b$ is used in conjunction with ΔV ; this imposes a limitation that V_{ex} must be less than ΔV . If V_{dc} exceeds V_b , then there will be a non-zero DCP even when the device is supposed to be in the quenched state. This results in a faster rise in DCP with increasing PDE. We see some evidence of this effect in the highest DCP data point in each of the three lowest curves in Figure 1. However, we have included these points to illustrate worst case DCP for PDE values on the order of 30%. Bias circuitry with larger ΔV would enable higher PDE.

Afterpulsing dependence on repetition rate

The demand for higher key throughput in QKD networks requires faster single photon counting rates. With SPADs, operation at faster repetition rates is hampered by a rate-dependent increase in the DCP. With each avalanche event, some fraction of the electrical carriers created will become trapped at defects in the multiplication region and will be thermally detrapped without consequence while the SPAD is in its quenched state. However, if a significant number of trapped carriers are still being detrapped when the gate is re-applied, then they can trigger a dark count and increase DCP. Shorter periods of time between gates will lead to a higher probability of dark counts induced by detrapped carriers. These dark counts which exceed the intrinsic (i.e., low repetition rate) DCP are generally referred to as "afterpulses."

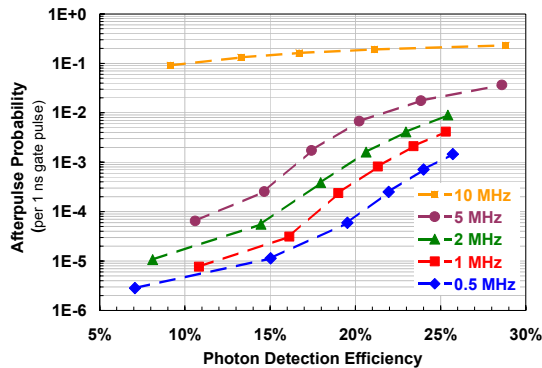


Figure 2: Afterpulse probability vs. PDE as a function of repetition rate.

In Figure 2, we present measurements of the probability of an afterpulse within a 1-ns gate as a function of PDE for a number of different repetition rates. For rates between 500 kHz and 5 MHz, the afterpulse probability (APP) at 10% PDE increases roughly proportionally with the repetition rate. At 5

MHz, the APP of $<10^{-4}$ at 10% PDE would generally be very good for QKD applications. However, for a 10 MHz rate, APP jumps dramatically—by nearly three orders of magnitude—for a PDE of 10%. This behavior indicates that for the operating conditions described, a detrapping time constant on the order of 0.1 μ s results in a drastic change in APP for a repetition rate increase from 5 MHz to 10 MHz.

Performance modeling

To gain a more comprehensive understanding of various trade-offs in SPAD performance, we have carried out extensive device modeling. Following the formalism in Ref. [4], we have computed DCP vs. PDE with the goal of identifying the dominant leakage mechanisms so that device performance can be optimized for various operating conditions.

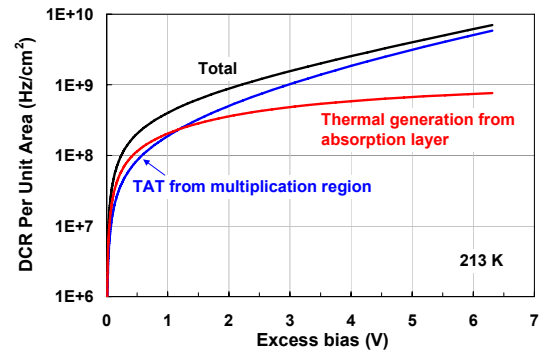


Figure 3: Modeling results for dominant dark count rate contributions vs. excess bias.

In Figure 3, we present modeling results showing the calculated dependence of the dark count rate per unit area on excess bias V_{ex} . Among all layers in the structure, dark carrier generation is dominated by (i) trap-assisted tunneling (TAT) in the InP multiplication region and (ii) thermal generation in the InGaAs absorption region. At 213K, these two mechanisms have comparable contributions for V_{ex} up to ~ 2 V; for higher voltages, the TAT mechanism dominates. At somewhat higher temperatures (e.g., 240 K), thermal generation dominates for $V_{ex} < 5$ V. These model results have guided the optimization of SPAD design for different operating conditions such as temperature, bias, and alternative operating wavelengths (e.g., 1.3 μ m and 1.06 μ m [5]).

References

- [1] M. A. Itzler, et al., J. Mod. Opt., vol. 54, p. 283 (2007).
- [2] S. Cova, et al., Appl. Opt., vol. 35, p. 1956 (1996).
- [3] D.S. Bethune, et al., J. Mod. Opt., vol. 51, p. 1359 (2004).
- [4] J.P. Donnelly, et al., IEEE J. Quantum Electron., vol. 42, p. 797 (2006).
- [5] X. Jiang, et al., IEEE J. Quantum Electron., vol. 44, p. 3 (2008).